

## Magnetic properties of polycrystalline $R_{1.5}\text{Ce}_{0.5}\text{Sr}_2\text{Cu}_2\text{NbO}_{10}$ ( $R = \text{Eu}, \text{Nd}, \text{and Sm}$ ) high- $T_c$ superconducting ceramics

M. Bennahmias and A. F. Bello

*Department of Applied Science, University of California, Davis-Livermore, Livermore, California 94550  
and Lawrence Livermore National Laboratory, Livermore, California 94550*

D. Back

*Lawrence Livermore National Laboratory, Livermore, California 94550*

H. B. Radousky

*Department of Physics, University of California, Davis, Davis, California 95616  
and Lawrence Livermore National Laboratory, Livermore, California 94550*

T. J. Goodwin, P. Klavins, and R. N. Shelton

*Department of Physics, University of California, Davis, Davis, California 95616  
(Received 22 March 1993; revised manuscript received 20 May 1993)*

Magnetic characterization has been performed on the superconducting members of the  $R_{1.5}\text{Ce}_{0.5}\text{Sr}_2\text{Cu}_2\text{NbO}_{10}$  ( $R = \text{Eu}, \text{Nd}, \text{and Sm}$ ) series. These materials are related to the  $\text{YBa}_2\text{Cu}_3\text{O}_{7-8}$  structure through the replacement of the  $\text{CuO}$  chains with  $\text{NbO}_2$  planes, and the single rare-earth elements with a  $R_2\text{O}_2$  fluorite structure. Measurements of the lower critical-field curve, irreversibility line, volume fraction, Meissner fraction, and magnetic relaxation are reported for each compound. No evidence of intergrain weak-link behavior down to 0.1 Oe is observed. Estimates of the zero-field intragrain critical current density from high-field hysteresis curves taken at 6 K for the Nd-, Sm-, and Eu-based systems are  $2.7 \times 10^4$ ,  $3.3 \times 10^4$ , and  $4.7 \times 10^4$  A/cm<sup>2</sup>, respectively.

### I. INTRODUCTION

Recent investigations by several groups<sup>1-13</sup> into developing cuprate high- $T_c$  superconductors have examined the effects of doping metallic titanium, niobium, and tantalum into the well characterized  $R\text{Ba}_2\text{Cu}_3\text{O}_7$  ( $R$  is a rare-earth element except Ce, Pr, and Tb) high- $T_c$  superconducting ceramics. Mattheiss<sup>1,2</sup> recently proposed that layered cuprate phases containing intermediate  $\text{TiO}_2$ ,  $\text{NbO}_2$ , and  $\text{TaO}_2$  electronic buffer layers could become superconducting if suitable doping of carriers could be achieved within these materials. Theoretical band-structure calculations for these compounds show distinct band features near the Fermi energy, namely a pair of half-filled, nearly degenerate antibonding  $\sigma^*$  subbands that are a well-known characteristic of the high- $T_c$  superconductor  $\text{YBa}_2\text{Cu}_3\text{O}_{7-8}$  (YBCO).<sup>1,2</sup>

Murayama *et al.*<sup>3</sup> successfully formed the tantalum-doped electrical insulating phase  $\text{LaBa}_2\text{Cu}_2\text{TaO}_8$  (LBCTO). Later work<sup>4-9</sup> showed that isostructural insulating niobium analogs  $R\text{Ba}_2\text{Cu}_2\text{NbO}_8$  ( $R = \text{La}, \text{Pr}, \text{and Nd}$ ) could also be formed. The structural analysis done in these studies on these  $R\text{Ba}_2\text{Cu}_2\text{MO}_8$  ( $M = \text{Ta}$  or  $\text{Nb}$ ) materials have shown that the RBCMO structure is derived from the RBCO tetragonal oxygen-deficient triple perovskite structure with  $\text{MO}_2$  ( $M = \text{Ta}$  or  $\text{Nb}$ ) planes preferentially replacing only the  $\text{CuO}$  chains, while leaving the  $\text{CuO}_2$  planes intact. Moreover determination of the lattice parameters for these RBCMO tetragonal

phases have demonstrated that the lattice mismatch between the parent RBCO orthorhombic phase to be <2% both normal to and along the  $\text{CuO}_2$  planes making these materials excellent candidates for epitaxially grown RBCO/RBCNO multilayer thin films. However, attempts at raising the Cu oxidation state in the  $\text{CuO}_2$  planes by doping holes into these RBCNO materials through chemical substitution such as  $\text{Ca}^{2+}$  and  $\text{Sr}^{2+}$  in for  $\text{La}^{3+}$  and  $\text{Ti}^{4+}$  in for  $\text{Nb}^{5+}$  have thus far been unsuccessful.

Li and co-workers<sup>10,11</sup> formed the compounds  $\text{Nd}_{1.5}\text{Ce}_{0.5}\text{Sr}_2\text{Cu}_2\text{MO}_{10}$  ( $M = \text{Nb}$  or  $\text{Ta}$ ). Cava *et al.*<sup>12</sup> later refined the preparation technique and were able to make  $\text{Nd}_{1.5}\text{Ce}_{0.5}\text{Sr}_2\text{NbO}_{10}$  (NdCSCNO) superconducting with a  $T_c$  of approximately 28 K. Recently, Goodwin, Radousky, and Shelton<sup>13</sup> were successfully able to form two additional isostructural cuprate-niobate superconducting phases  $R_{1.5}\text{Ce}_{0.5}\text{Sr}_2\text{Cu}_2\text{NbO}_{10}$  ( $R = \text{Eu}$  and  $\text{Sm}$ ) with a  $T_c$  of 25 and 28 K, respectively. Rietveld refinement analysis<sup>10,11</sup> of the crystallographic structure of these RCSCNO cuprate niobates from powder x-ray-diffraction data taken during these studies show that in addition to local substitution of  $\text{NbO}_2$  planes for the  $\text{CuO}$  chains in the RBCO structure, a fluorite structured  $(R_{1.5}\text{Ce}_{0.5})\text{O}_2$  layer fully replaces the rare-earth layer, while strontium atoms are substituted in for the barium atoms. The RCSCNO  $T'$  phase crystallographic structure is shown in Fig. 1.

In this paper, we report on the static and dynamic

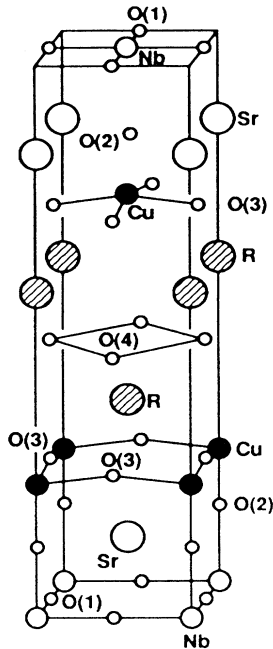


FIG. 1. The RCSCNO  $T'$  phase crystallographic structure. Oxygens in the Nb, Sr, and Cu layers are designated as O(1) or O(5), O(4), and O(2) or O(3), respectively, while O(4) denotes the oxygens between the fluorite layers.

behavior of the superconducting members of the cuprate-niobate  $R_{1.5}Ce_{0.5}Sr_2Cu_2NbO_{10}$  ( $R = \text{Eu, Nd, and Sm}$ ) family of compounds in external magnetic fields. Measurements of the volume fraction, the Meissner fraction, the lower critical-field curve, and dc irreversibility phase line are reported. The Bean critical state model is used to extract values for the zero-field critical current densities in these materials. The field and temperature dependence of the magnetic relaxation rates in these cuprate-niobate materials are also presented. The discussion covers the issue of observing superconductivity in other members of the homologous series  $(R, \text{Ce})_{1+n}Sr_2Cu_2NbO_{8+2n}$  ( $R = \text{Nd, Sm, and Eu}$ ) and discusses the observed temperature and field dependence of the relaxation rates in these materials within the framework of a distribution of activation energies.

## II. EXPERIMENT DETAILS

Polycrystalline samples of RCSCNO were prepared by conventional solid-state reaction methods. Stoichiometric amounts of high purity (99.99% or better)  $\text{CeO}_2$ ,  $\text{Nd}_2\text{O}_3$ ,  $\text{Sm}_2\text{O}_3$ ,  $\text{Eu}_2\text{O}_3$ ,  $\text{SrCO}_3$ ,  $\text{CuO}$ , and  $\text{Nb}_2\text{O}_5$  powders were appropriately weighted, ground together, and pressed into  $\frac{3}{8}$ -in. pellets. The finished pellets were placed in alumina crucibles and sintered at  $1120^\circ\text{C}$  for 80 h in a slightly pressurized (approximately 30 kPa) oxygen atmosphere and then allowed to furnace cool to room temperature. The lengthy anneal time was required to allow sufficient time for the appropriate Cu and Nb cation ordering to occur within the structure. Samples were then reground, pressed into pellets, and the firing process

repeated. Subsequent powder x-ray-diffraction data were taken on each of the samples, validating the formation of the expected phase, the results of which have been previously described elsewhere.<sup>13</sup>

A commercially available SEMCO Nanolab 7 high-resolution scanning electron microscope (SEM) was used to obtain an image of the bulk morphology of each of the sintered materials in order to estimate the average size and shape of the superconducting grains. In each case the sintered specimen was ground to a fine powder prior to use in the SEM.

The magnetization data were all taken on a commercially available Quantum Design rf superconducting quantum interference device (SQUID) magnetometer. Zero-field cooled and field-cooled dc magnetization profiles over the temperature range 5–60 K were obtained for each compound for magnetic fields ranging from 5 to 10 000 Oe. Hysteresis data for each compound were taken at 6, 15, 23, and 30 K for magnetic field excursions of  $\pm 5$ ,  $\pm 20$ ,  $\pm 50$ ,  $\pm 100$ ,  $\pm 500$ , and  $\pm 55\,000$  Oe. Partial isothermal magnetization curves, used in determining lower critical-field estimates for each of the materials, were taken at several different temperatures ranging from 5 to 25 K and a magnetic-field sweep of 0 to 90 Oe. Estimates of the effective magnetic moment from low-field susceptibility profiles were obtained for each of the samples over the temperature range of 30–300 K in a magnetic field of 5000 Oe. Zero-field-cooled and field-cooled magnetic relaxation data were obtained for applied magnetic fields of 50, 500, 1000, and 5000 Oe at several temperatures in the range of 4.5–30 K.

## III. EXPERIMENTAL RESULTS

The mass of the SmCSCNO, NdCSCNO, and EuCSCNO test pieces that were used throughout this study were measured to be  $0.0702 \pm 0.0005$ ,  $0.0875 \pm 0.0005$ , and  $0.0195 \pm 0.0005$  g, respectively. The experimental densities of the RCSCNO sintered samples were measured to be approximately 92% of their theoretical densities. The measured densities of the RCSCNO ceramics were higher than expected considering the powder sintering methods employed. Notably, Peng, Shelton, and Radousky<sup>14</sup> have measured equally high-density yields of 90% or greater for sintered  $\text{Nd}_{2-x}\text{Ce}_x\text{CuO}_{4-\delta}$  phases embodying a similar fluorite-type layer structure suggesting that these types of materials tend to sinter well. The SEM results showed that the superconducting grains in these polycrystalline RCSCNO samples were irregularly shaped with very rough surfaces. The average grain size from these SEM images was estimated to be approximately  $10\ \mu\text{m}$  in diameter.

The temperature variation of the slope  $dM/dH$ , in the diamagnetic region, from a number of low-field hysteresis runs taken at several temperatures was examined. The temperature dependence of the slope  $dM/dH$  in the diamagnetic regime is a convolution of the temperature-dependent superconducting volume fraction and the temperature-independent demagnetization factor. Figure 2 shows the temperature dependence of the slopes  $dM/dH$  for all three RCSCNO samples. At the lower

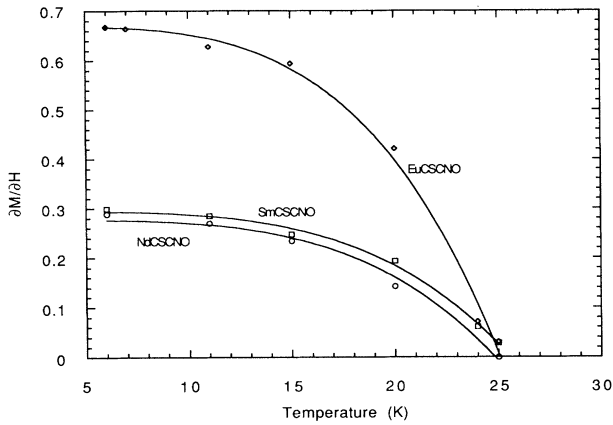


FIG. 2. The slope  $\partial M/\partial H$  evaluated in the linear diamagnetic region as a function of temperature for the three RCSCNO materials. The lines shown in this figure are curve fits to the expression  $A[1-(T/T_c)^4]$ .

temperatures the value of the slope can be readily observed to saturate indicating that a maximum in the superconducting volume fractions in these ceramics have been obtained, while at the higher temperatures, near the transition temperature, the slope drops to zero. The behavior of the slope  $dM/dH$  with respect to temperature can be understood within the theoretical framework<sup>15-18</sup> developed for describing granular high- $T_c$  ceramics as a continuous medium with an effective permeability  $\mu_{cer}$  defined by

$$\mu_{cer} = f_n + f_s \langle \mu_g \rangle, \quad f_n + f_s = 1, \quad (1)$$

where  $f_s$  represents the volume fraction of superconducting grains,  $f_n$  is the amount of nonstoichiometric material, and  $\langle \mu_g \rangle$  is an averaged permeability of the superconducting grains defined by

$$\langle \mu_g \rangle = \theta_s / \theta_n, \quad (2)$$

with  $\theta_s$  and  $\theta_n$  being the flux penetrating into the grains under superconducting and normal conditions, respectively. In this interpretation, the temperature variation of  $\mu_{cer}$  is completely determined by the temperature dependence of the effective penetration depth into these ceramics by an external magnetic field. In the case of well sintered ceramics where the grains are extremely well connected, i.e., no weak links, the penetration depth is expected to be an intrinsic property of the superconducting grains as the flux can leak into the bulk material through the grain boundaries. As a guide for the reader the lines shown in Fig. 2 are curve fits to the expression  $A[1-(T/T_c)^4]$  where  $A$  is a fit parameter. The overall broad shape of these curves is believed to be a result of the inhomogeneity, or low volume fractions, of these granular materials whereas for granular materials with 100% volume fractions, or single crystals, the temperature variation of the slope  $dM/dH$  should be constant up to the critical temperature where it should then undergo an abrupt transition to zero.

An estimate of the superconducting volume fractions

at the low temperatures for each of the RCSCNO sintered materials was made using test samples from the same batch of compounds the original specimens were obtained from. These new samples were formed into "thin disks" so that the demagnetization factors could be easily estimated and the samples were subsequently zero-field cooled, introduced to a 20-Oe field, and the induced magnetization signal measured. The demagnetization factors for the irregularly shaped test specimens were then determined from the ratio of the volume fractions obtained in this way over the saturated value of the slope  $dM/dH$  at the low temperatures. Using this approach the average demagnetization factors  $N_{avg}$  obtained for the Nd-, Sm-, and Eu-based RCSCNO phases were  $0.10 \pm 0.01$ ,  $0.06 \pm 0.01$ , and  $0.22 \pm 0.01$ , respectively. The reader should take note that these demagnetization factors have been taken into account in the results that follow.

The results of a sequence of isothermal low-field hysteresis runs at 6 K obtained for the SmCSCNO phase are shown in Fig. 3. Similar data sequences were also generated for both the NdCSCNO and EuCSCNO compounds. There appears to be no observable weak-link behavior down to 0.1 Oe, the lowest attainable field in the SQUID. Typically, the presence of weak links will be made clear by the opening of a small rectangular inner hysteresis loop at sufficiently low magnetic-field excursions ( $< 1$  Oe) that closes again at somewhat higher magnetic fields ( $> 10$  Oe).<sup>17,19-21</sup> To explore the possibility that weak-link behavior in these materials might be observable at higher temperatures, where the contribution of this effect to the overall magnetization signal would most likely begin to dominate over that from the persistent supercurrents, additional low-field hysteresis data were also taken at 15 and 23 K on these Sm-, Eu-, and Nd-based RCSCNO compounds. Subsequent examination of the results indicated that no weak-link behavior was observed to occur even at these elevated temperatures. The absence of any noticeable weak links in these

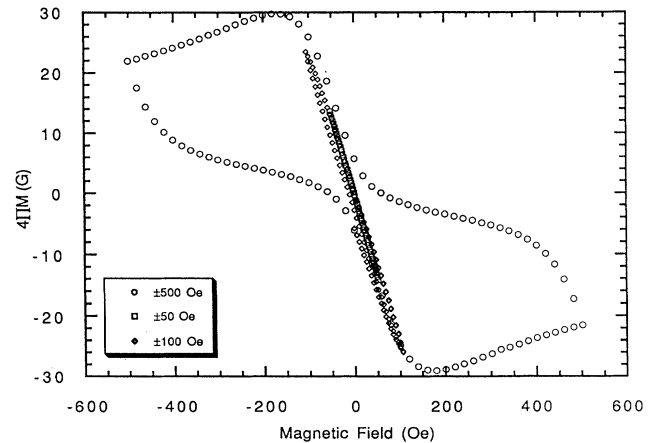


FIG. 3. A set of low-field hysteresis data taken on the SmCSCNO sample for magnetic-field excursions of (a)  $\pm 50$ ,  $\pm 100$ , and  $\pm 500$  Oe and (b)  $\pm 5$  and  $\pm 20$  Oe. No secondary loop at the low fields due to weak-link behavior was observed in the data.

high-density sintered RCSCNO materials, at least at the magnetic fields used in this study, suggests that the magnetization is primarily due to the superconducting grains.

Several experimental data points illustrating the magnetic-field dependence of the zero-field-cooled (ZFC) shielding ratio of the three RCSCNO compounds are shown in Fig. 4. The ZFC shielding ratio for each test specimen was obtained by dividing the maximum difference in the values of the ZFC magnetization curve by the applied magnetic field accounting for demagnetization effects. Figure 4 shows that the ZFC shielding ratios for these materials are constant for sufficiently low fields but begin to decrease at the higher-field strengths indicating the onset of flux penetration. This type of behavior, attributed to the grain boundaries being the reversible paths of the flux lines, has been previously observed by Kitazawa *et al.*<sup>22</sup> in polycrystalline  $\text{Bi}_2\text{Sr}_2\text{CaCu}_2\text{O}_8$  (BSSCO) where these sintered test specimens responded like a powder under the influence of high magnetic fields but like a single crystal in the low magnetic-field regions having nearly a flat response in the intermediate field range. Notably, the volume fractions for the Nd-, Sm-, and Eu-based RCSCNO materials estimated from the ZFC shielding ratio at the low fields were 16, 30, and 42%, respectively.

The magnetic-field dependence of the field-cooled (FC) shielding ratio in these RCSCNO samples shows a similar field dependence to the ZFC shielding ratios. The Meissner fractions were obtained in an analogous fashion to the volume fractions with the FC magnetization curves used instead. The results for the Meissner fractions for the Nd-, Sm-, and Eu-based RCSCNO materials were 10, 20, and 19%, respectively. The rapid decrease in both the ZFC and FC shielding ratios for the Nd-based analog is attributed to poor phase purity. The FC shielding ratio is much less than the corresponding ZFC shielding ratio for these RCSCNO compounds. The origin of this difference between the ZFC shielding ratio and FC shielding ratio for high- $T_c$  materials can be explained on the basis of flux pinning. At the smaller fields, the ZFC

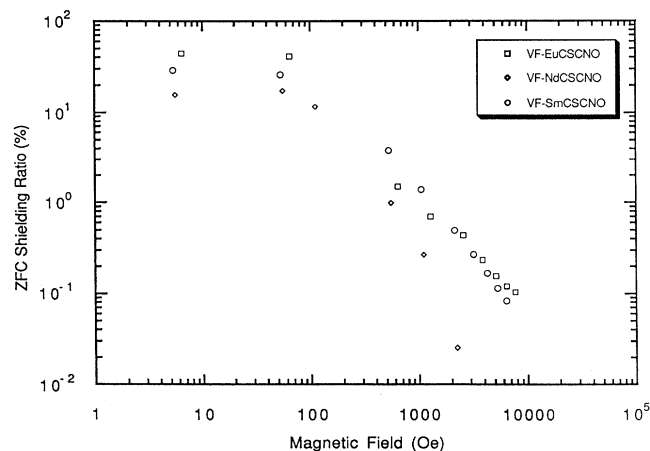


FIG. 4. The ZFC shielding ratio for the three RCSCNO compounds plotted vs magnetic field. The FC shielding ratio for the three RCSCNO compounds plotted vs magnetic field shows a similar field dependence.

and FC magnetization signals tend to be nearly the same because the ZFC samples exhibit full flux expulsion and very little flux is trapped within the field-cooled samples. For intermediate fields, due to increased trapping of flux within the grains, ZFC magnetization signals tend to be greater than FC magnetization signals. Finally, for high fields, due to a reduction in flux expulsion from the ZFC samples, the Meissner fraction and volume fraction become nearly equal; their ratio eventually becoming unity.

A representative set of magnetization versus field data, obtained at various different temperatures that were measured for each of the RCSCNO samples. The field of first vortex entry (flux trapping) into the grains was chosen to be the field where the magnetization data at a given temperature began to reasonably deviate from linearity ( $<0.999$  in goodness-of-fit values). The results of estimating the lower critical field  $H_{c1}$  versus temperature is shown in Fig. 5. These results tend to agree well with the fields at which the onset of a reduction in the ZFC shielding ratio for these RCSCNO specimens is observed to happen. Moreover, the  $H_{c1}$  results also agree with the fields at which the onset of flux trapping occurs in these materials as determined from the low-field hysteresis data. The temperature behavior of the  $H_{c1}$  lines do not show any indication of saturation at low temperatures as might be expected for intrinsic BCS-type behavior.<sup>23</sup> Similar behavior in the temperature dependence of  $H_{c1}$  has been previously observed in magnetization studies on oriented polycrystals of RBCO.<sup>24,25</sup>

The results of high-field hysteresis runs taken at 6 K for the three RCSCNO samples suggest that they are a convolution of a large positive magnetization, attributable to the strong  $4f$  electron interactions of the magnetic rare-earth ions in these materials, and an underlying hysteretic behavior characteristic of type-II superconductors. At the higher magnetic fields a saturation in the magnetization signal can be observed to occur in the NdCSCNO system. Similar saturation effects have been previously observed in high-field magnetization data taken on polycrystalline NdBCO.<sup>26</sup> On the other hand, the

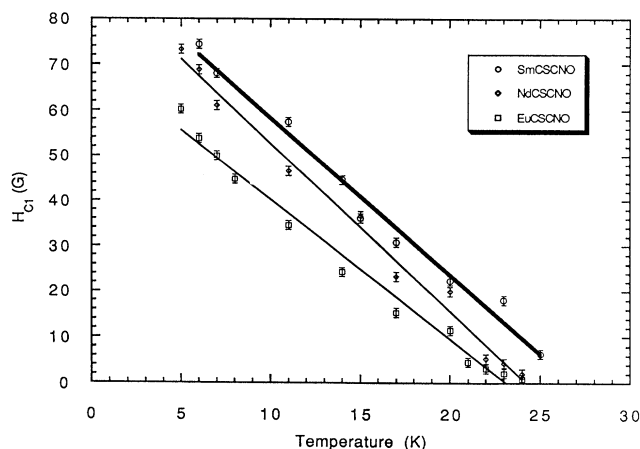


FIG. 5. The  $H_{c1}$  lines plotted as a function of temperature for all three RCSCNO materials. The error bars in obtaining the values of  $H_{c1}$  in these materials is estimated to be  $\pm 1$  G.

field dependence of the magnetization signal remains fairly linear in both the Sm- and Eu-based RCSCNO systems. Due to crystalline-field effects, the paramagnetic response of these  $4f$  electron systems cannot be described by a simple Brillouin function and therefore the positive magnetization component cannot be easily subtracted out from the overall signal. As a result, estimates for the upper critical field  $H_{c2}$  for the RCSCNO compounds from the high-field hysteresis data were not possible. Still it is often useful to gain a physical feeling for the relative strength of the magnetic interactions, i.e., saturation moments, in these RCSCNO compounds by attempting to fit the high-field hysteresis data to a Brillouin function at least for temperatures above  $T_c$ . An upper bound on the saturation moments at 30 K for the Nd- and Sm-based RCSCNO compounds using this method were roughly  $4.86\mu_B$  and  $1.11\mu_B$ , respectively. These values appear to be reasonable in light of the  $\mu_{\text{eff}}$  values of 2.97 and 0.42 previously reported from low-field susceptibility data.<sup>13</sup>

A set of ZFC and FC magnetization data taken for the NdCSCNO system at 5, 100, 1000, and 2000 Oe is shown in Fig. 6. The magnitude of the 2000-Oe ZFC and FC data have been reduced by a factor of 5 and that of the 100-Oe data by a factor of 3 in order to make it easier to compare the inherent features of all the curves over the broad range of fields used. A strong paramagnetic contribution at the higher fields in both the zero-field and field-cooled magnetization signals causes a noticeable upturn at low temperatures.

The irreversibility phase lines for the three RCSCNO test specimens are shown in Fig. 7. The data points comprising the irreversibility phase curves were obtained by determining the point of departure of the FC signal from the ZFC signal as a function of the applied magnetic field. The irreversibility lines were subsequently fit to a “quasi-de Almeida-Thouless” relationship of the form<sup>27–31</sup>

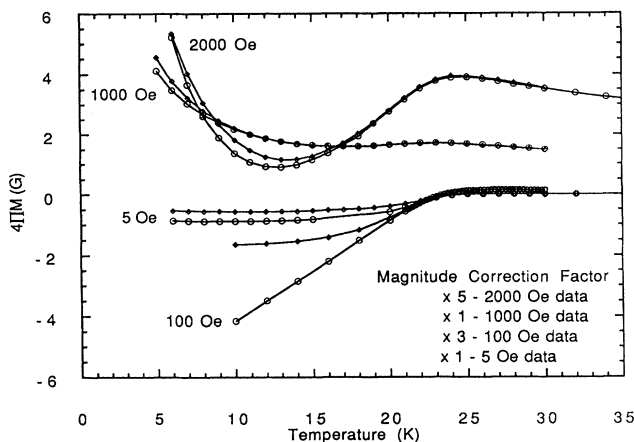


FIG. 6. Zero-field-cooled and field-cooled magnetization signals as a function of temperature taken on the NdCSCNO specimen for fields of 5, 100, 1000, and 2000 Oe. The magnitude of the 2000-Oe data has been reduced by a factor of 5 and that for the 100-Oe data by a factor of 3 for clarity. A strong paramagnetic contribution to these data, from  $4f$  interactions between the rare-earth ions, can be seen.

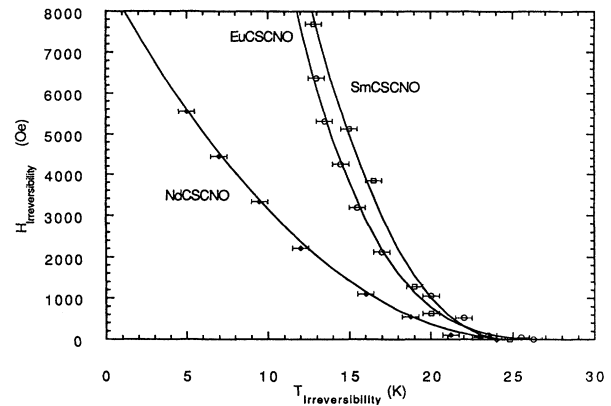


FIG. 7. The  $H$ - $T$  irreversibility phase lines for the three RCSCNO materials. The lines shown in this figure are quasi-de Almeida-Thouless curve fits to the data. The error in the values of  $T_{\text{irr}}$  are estimated to be  $\pm 0.5$  K.

$$H(T_{\text{irr}}) = H(0)[1 - (T_{\text{irr}}(H)/T_{\text{irr}}(0))]^n, \quad (3)$$

where  $T_{\text{irr}}$  is the irreversibility temperature. Table I provides the values of  $H(0)$ ,  $T_{\text{irr}}(0)/T_c$ , and  $n$  obtained from the curve fits for the EuCSCNO, SmCSCNO, and NdCSCNO samples.

The results shown in Fig. 7 agree reasonably well with the temperature dependence of the magnetic field that separates the reversible and irreversible paths in the high-field hysteresis data for these samples. Notably, the large values for  $t \sim 0.91$ – $1.02$  may indicate that the phase boundary between the reversible and irreversible behavior in these RCSCNO materials might closely coincide with the critical phase line  $T_c(H)$ . Resistivity measurements on these RCSCNO compounds to determine the upper critical field are needed to verify this. Additional work is also being performed to determine the differences that arise in determining the irreversibility lines for these materials by taking FC measurements during a warming cycle versus a cooling cycle. It is expected that these hysteresis differences would be much less pronounced in these materials than in YBCO due to the small  $T_c$ .

In lieu of electrical transport measurements, the magnetic-field dependence of intragrain critical current densities are often deduced from hysteresis data where the irreversible behavior is assumed to be related to flux expulsion from the persistent supercurrents flowing around the grain boundaries. For most polycrystalline high- $T_c$  materials the Bean critical state model (CSM) really only provides a rough estimate of the intragrain

TABLE I. Quasi-de Almeida-Thouless fit parameters for RCSCNO ( $R = \text{Nd, Eu, and Sm}$ ).

| Compound | $H(0)$ [kOe] | $k = T_{\text{irr}}(0)/T_c$ | $n$  |
|----------|--------------|-----------------------------|------|
| NdCSCNO  | 8.77         | 0.91                        | 2.05 |
| EuCSCNO  | 51.71        | 0.99                        | 3.07 |
| SmCSCNO  | 48.27        | 1.02                        | 3.31 |

critical current density,  $J_c(H, T)$ , because the magnetic-field dependence is neglected and hence the magnetization at which the flux penetrates to the center of a sample depends on the temperature. According to the Bean model  $J_c$  [A/cm<sup>2</sup>] is given by the relationships<sup>32–34</sup>

$$J_c = 15 \cdot \Delta M / R, \quad (4)$$

where  $\Delta M$  [emu/cm<sup>3</sup>] is the width of the hysteresis loop and  $R$  [cm] is the average radius of the grains. It should be noted that the value of the zero-field critical current density  $J_c(0, T)$  determined by this method will depend on the accuracy from which the average grain size and overall shape can be determined, i.e., the model assumes cylindrical symmetry. The zero-field current density is an important intrinsic material parameter for polycrystalline superconductors because it describes the transport characteristics of the superconducting grains in the absence of any fields. The critical current densities for the NdCSCNO, SmCSCNO, and EuCSCNO compounds estimated using the Bean critical state model are plotted in Fig. 8 as a function of magnetic field for a temperature of 6 K. The critical current density is observed to be the highest in the Eu analog indicating that a greater amount of flux trapping occurs within this material. This seems reasonable in light of the  $H_{c1}$  results previously discussed. From Fig. 8, the estimates of the  $J_c(0, 6 \text{ K})$  values for the Eu-, Sm-, and Nd-based RCSCNO systems are  $\sim 4.7 \times 10^4$ ,  $3.3 \times 10^4$ , and  $2.7 \times 10^4$  A/cm<sup>2</sup>, respectively. These numbers are similar to those reported for sintered TBCCO (Ref. 18) within one order of magnitude of those originally reported for sintered BSSCO (Ref. 35) and two orders of magnitude smaller than sintered YBCO.<sup>36–38</sup>

A set of ZFC magnetic relaxation data versus time at different temperatures were generated for the NdCSCNO, SmCSCNO, and EuCSCNO materials. FC magnetic relaxation data were also taken for these compounds but as no measurable changes occurred in any of the FC samples, i.e., the magnetization signal remained constant, the results from these experiments have not been included. An analysis of the time dependence of the

decay of the ZFC magnetization signals by plotting these values versus the logarithm of the time at which each experimental data point was measured showed this relationship to be linear. This logarithmic decay in time can be related to a thermally activated vortex creep process in which flux lines in the critical state hop over potential barriers due to thermal activation.<sup>39–41</sup> Assuming a single-barrier height  $U_0$  (activation energy) for the pinning centers, the decay in magnetization signals were fit to the well-known relationship

$$M(H, T) = M(H, 0) [1 - (kT/U_0) \ln(1 + t/\tau)], \quad (5)$$

where  $t$  is the measurement time and  $\tau$  is the relaxation time for the flux line to jump over the pinning well. The value of  $\tau$  that was used in these calculations was  $10^{-9}$  sec and the experimental times for these measurements ranged from 1 up to  $10^4$ – $10^5$  sec. The results of extracting  $U_0$  as a function of temperature for the three RCSCNO materials is shown in Fig. 9 at 500 Oe. The values for the single-barrier activation energies in the RCSCNO compounds are observed to range from 0.02 to 0.66 eV. The magnitude of these pinning well depths is considerably smaller than the single-barrier activation energies previously reported for sintered YBCO  $\sim 1$  to 1.5 eV.<sup>35</sup> This may simply be a consequence of the lower  $T_c$  in these materials. In order to determine the nature of the field dependence of the magnetic relaxation in these compounds, a set of relaxation measurements were made at 6 K for several different fields. A definite peak in the values for the relaxation rates can be clearly seen for all three RCSCNO compounds. Figure 10 also shows that the character of the field dependence on either side of this peak are not the same. This type of asymmetric relaxation behavior has also been observed for other granular high- $T_c$  superconductors.<sup>30,39</sup> Preliminary evaluation of the overall shape of these relaxation rate data show that the nature of the curve for low fields has a quadratic dependence on magnetic-field strength. A preliminary comparison with theoretical predictions<sup>42,43</sup> for the relaxation rate profiles generated from various CSM suggest

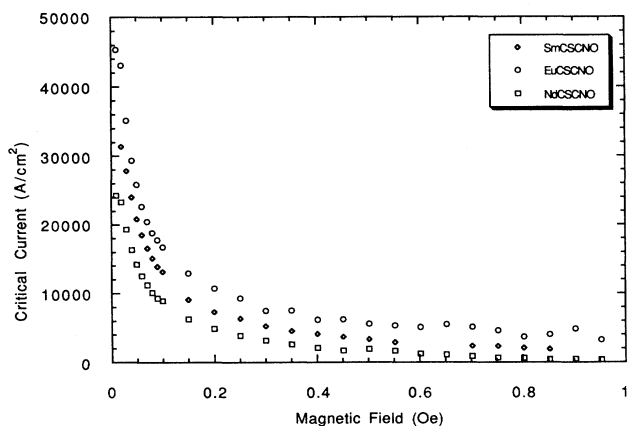


FIG. 8. Critical current density profiles deduced from the Bean CSM for the RCSCNO compounds plotted as a function of magnetic field.

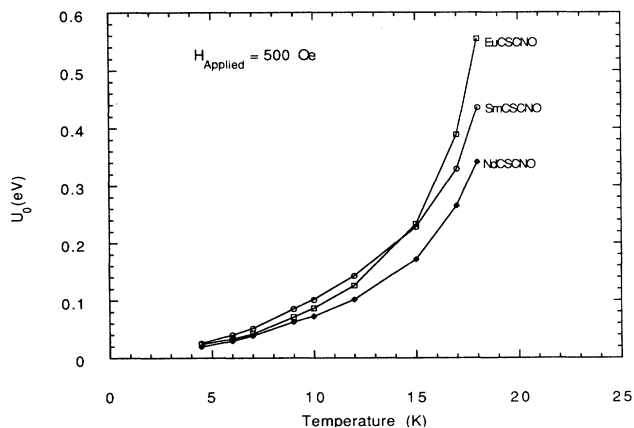


FIG. 9. Single-barrier activation energies plotted as a function of temperature for the Nd-, Sm-, and Eu-based RCSCNO compounds for an applied magnetic field of 500 Oe.

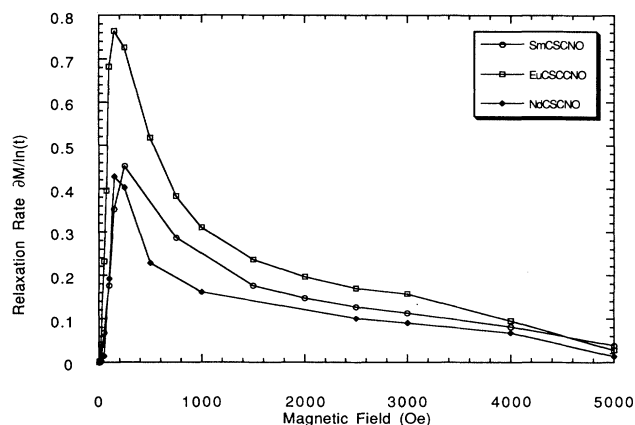


FIG. 10. The magnetic relaxation rates for the Nd-, Sm-, and Eu-based RCSCNO test samples plotted as a function of the applied magnetic field. The asymmetric dependence of the relaxation rate on the applied field on either side of the peak can be clearly seen.

that the critical state for these cuprate-niobate samples might be described by either the exponential decay CSM or the inverse linear polynomial CSM. Moreover, while an  $H^2$  dependence is correctly predicted for low fields, comparison with the Bean CSM predictions for the higher fields indicates that the complex behavior in these RCSCNO materials is not properly accounted for within the framework of this model. Additional work to determine the appropriate critical state framework to interpret the magnetic relaxation behavior in these particular high- $T_c$  superconductors would prove beneficial.

#### IV. DISCUSSION

A simple application of the bond valence sum technique<sup>44</sup> to estimate the excess charge concentration in the  $\text{CuO}_2$  planes for the Nd-, Sm-, and Eu-based RCSCNO phases yields 2.3224, 2.3032, and 2.3203, respectively. These results indicate that the  $\text{CuO}_2$  planes are in fact overdoped with holes. This is in sharp contrast to the  $R_{1.85}\text{Ce}_{0.15}\text{CuO}_{4-\delta}$  ( $R = \text{Pr, Nd, Eu, and Sm}$ ) system where Hall measurements<sup>45</sup> have shown the electrons to be the charge carriers responsible for the high-temperature superconductivity. Interestingly, Matheiss<sup>1</sup> has pointed out that if the appropriate level of Ce doping could be achieved, other phases in the homologous series  $(\text{Nd,Ce})_{1+n}\text{Sr}_2\text{Cu}_2\text{NbO}_{8+2n}$ , in which the individual members contain fluorite blocks with different thicknesses, could also be made superconducting. The doping of Ce should also lead to discovery of superconductivity in the corresponding Eu- and Sm-based homologous series.

The two best recognized physical pictures that have been previously used to describe the essential features of both dynamic and static magnetic interactions in granular high- $T_c$  ceramics are (1) a superconducting "spin-glass" model (Refs. 15–21, 27, 28, 35–38, and 46–48) based on the dynamics of a disordered ensemble of weakly coupled anisotropic superconducting grains separated

by nonstoichiometric material and (2) a thermally activated flux-creep and flux-flow model based on the strength of pinning forces and local vortex-field gradients (Refs. 22, 29, 30, 31, 39, and 49–61). The bulk of the experimental data currently available on granular high- $T_c$  compounds have been interpreted equally well within the framework of either model. The experimental results of the magnetic behavior for these high- $T_c$  cuprate-niobate materials similarly do not provide sufficient evidence that would tend to favor the spin-glass model over the flux-creep model or vice-versa. The presence of weak links at smaller fields in these materials cannot be entirely ruled out. Furthermore, some of the data such as the irreversibility phase lines lend themselves more easily to a spin-glass description, while the magnetic relaxation and critical current densities are better understood in terms of flux pinning and vortex gradients. Still other measurements like the lower critical field curves can be understood equally well in either physical model. Experimental data on single crystals of these RCSCNO materials would certainly assist in providing information that might help to provide additional insight into the physical mechanisms of the magnetic behavior for these niobium-doped superconductors.

Lastly, if the single-barrier thermally activated flux-creep scenario governed the process of magnetic relaxation in these high- $T_c$  systems, then one might expect that each individual pinning well depth would decrease to zero with increasing temperature so that  $U_0(T_c) = 0$ , since the material would no longer be superconducting and the magnetic flux should fully be able to penetrate into the bulk. One of the surprising features in the magnetic relaxation data obtained for high- $T_c$  materials is that the activation energies at some magnetic fields can actually increase with increasing temperature, while for other fields the activation energies can even show several peaks. This unusual behavior for high- $T_c$  materials has been explained<sup>30</sup> on the basis of the presence of a distribution of activation energies in these materials rather than simply a single-barrier height that is uniform throughout the sample. For low temperatures the observed decay rate is due to the low activation energies and at higher temperatures only the surviving deep wells contribute to the decay of the magnetization signals. This approach has already proved successful in describing similar effects in  $R_{1.85}\text{Ce}_{0.15}\text{CuO}_{4-\delta}$  samples<sup>30</sup> as well as BSSCO samples.<sup>41</sup> Additional work incorporating an inversion scheme<sup>40</sup> proposed to obtain the distribution function of activation energies for these cuprate-niobate materials needs to be performed.

#### ACKNOWLEDGMENTS

Work at Lawrence Livermore National Laboratory and UC-Davis was performed under the auspices of the U.S. Department of Energy under Contract No. W-7405-ENG-48. Part of the work done at UC-Davis was supported by the National Science Foundation under Grant No. DMR-90-21029 and the Air Force under Grant No. F49620-92-J-0514.

- <sup>1</sup>L. F. Matheiss, *Phys. Rev. B* **46**, 11 171 (1992).
- <sup>2</sup>L. F. Matheiss, *Phys. Rev. B* **45**, 2442 (1992).
- <sup>3</sup>N. Murayama, E. Sudo, K. Kani, A. Tsuzuki, S. Kawakami, D. M. Awano, and Y. Torii, *Jpn. J. Appl. Phys.* **27**, L1623 (1988).
- <sup>4</sup>M. J. Rey, P. H. Dehault, J. Joubert, and A. W. Hewat, *Physica C* **167**, 162 (1990).
- <sup>5</sup>M. Bennaahmias, J. C. O'Brien, H. B. Radousky, T. J. Goodwin, P. Klavins, J. M. Link, C. A. Smith, and R. N. Shelton, *Phys. Rev. B* **46**, 11 986 (1992).
- <sup>6</sup>H. B. Radousky, J. C. O'Brien, M. Bennaahmias, P. Klavins, C. A. Smith, J. M. Link, T. J. Goodwin, and R. N. Shelton, in *Layered Superconductors: fabrication, properties, and applications*, edited by D. T. Shaw, C. C. Tsui, T. R. Schneider, and Y. Shioara, MRS Symposia Proceedings No. 275 (Materials Research Society, Pittsburgh, 1992), p. 113.
- <sup>7</sup>N. Rosov, J. W. Lynn, H. B. Radousky, M. Bennaahmias, T. J. Goodwin, P. Klavins, and R. N. Shelton, *Phys. Rev. B* **47**, 15 256 (1993).
- <sup>8</sup>C. Greaves and P. R. Slater, *Physica C* **161**, 245 (1989).
- <sup>9</sup>A. Ichinose, T. Wada, H. Yamauchi, and S. Tanaka, *J. Ceram. Soc. Jpn. Int. Ed.* **97**, 1053 (1989).
- <sup>10</sup>R. Li, Y. Zhu, Q. Qian, and Z. Chen, *Physica C* **176**, 19 (1991).
- <sup>11</sup>R. Li, Y. Zhu, C. Xu, Y. Qian, Z. Chen, and C. Fan, *J. Solid State Chem.* **94**, 206 (1991).
- <sup>12</sup>R. J. Cava, J. J. Krajewski, H. W. Zandbergen, R. B. Dover, W. F. Peck, Jr., and B. Hessen, *Physica C* **191**, 237 (1992).
- <sup>13</sup>T. J. Goodwin, H. B. Radousky, and R. N. Shelton, *Physica C* **204**, 212 (1992).
- <sup>14</sup>J. L. Peng, R. N. Shelton, and H. B. Radousky, *Solid State Commun.* **71**, 479 (1989).
- <sup>15</sup>John R. Clem, B. Bumble, S. I. Raider, W. J. Gallagher, and Y. C. Shih, *Phys. Rev. B* **35**, 6637 (1987).
- <sup>16</sup>John R. Clem, *Physica C* **153-155**, 50 (1988).
- <sup>17</sup>H. Dersch and G. Blatter, *Phys. Rev. B* **38**, 11 391 (1988).
- <sup>18</sup>R. Navarro, F. Lera, A. Badia, C. Rillo, J. Bartolome, W. L. Lechter, and L. E. Toth, *Physica C* **183**, 73 (1991).
- <sup>19</sup>P. Chaddah, G. Ravi Kumar, A. K. Grover, C. Radhakrishnamurthy, and G. V. Subba Rao, *Cryogenics* **29**, 907 (1989).
- <sup>20</sup>S. Senoussi, S. Hadjoudj, R. Maury, and A. Fert, *Physica C* **165**, 364 (1990).
- <sup>21</sup>S. Senoussi, M. Oussena, and S. Hadjoudj, *J. Appl. Phys.* **63**, 4176 (1988).
- <sup>22</sup>K. Kitazawa, Y. Tomioka, T. Hasegawa, K. Kishio, M. Naito, T. Matsushita, I. Tanaka, and H. Kojima, *Cryogenics* **31**, S35 (1991).
- <sup>23</sup>A. Umezawa, G. W. Crabtree, K. G. Vandervoort, U. Welp, W. K. Kwok, and J. Z. Liu, *Physica C* **162-164**, 733 (1989).
- <sup>24</sup>J. P. Strobel, A. Thoma, B. Hensel, H. Adrian, and G. Saemann Ischenko, *Physica C* **153-155**, 1537 (1988).
- <sup>25</sup>Y. Ishikawa, K. Mori, K. Kobayashi, and K. Sato, *Physica C* **153-155**, 1471 (1988).
- <sup>26</sup>J. Sebak, J. Stehno, V. Nekvasil, S. Safrata, L. Havelax, P. Svobodax, V. Valvodax, V. Sechovsky, J. Sramek, and K. Hruska, *Physica C* **153-155**, 186 (1988).
- <sup>27</sup>I. Morgenstern, K. A. Muller, and J. G. Bednorz, *Physica C* **153-155**, 59 (1988).
- <sup>28</sup>H. Keller, B. Pumpin, W. Kundig, W. Odermatt, B. D. Patterson, J. W. Schneider, H. Simmler, S. Connell, K. A. Muller, J. G. Bendorz, K. W. Blazey, I. Morgenstern, C. Rossel, and I. M. Savic, *Physica C* **153-155**, 71 (1988).
- <sup>29</sup>K. G. Vandervoort, U. Welp, J. E. Kessler, H. Claus, G. W. Crabtree, W. K. Kwok, A. Umezawa, B. W. Veal, J. W. Downey, and A. P. Paulikas, *Phys. Rev. B* **43**, 13 042 (1991).
- <sup>30</sup>C. C. Almasan, C. L. Seaman, Y. Dalichaouch, and M. B. Maple, *Physica C* **174**, 93 (1991).
- <sup>31</sup>A. K. Gangopadhyay, U. Balachandran, and R. B. Poeppel, *Physica C* **201**, 6 (1992).
- <sup>32</sup>G. Ravi Kumar and P. Chaddah, *J. Supercond.* **2**, 247 (1989).
- <sup>33</sup>G. Ravi Kumar and P. Chaddah, *Phys. Rev. B* **39**, 4704 (1989).
- <sup>34</sup>C. P. Bean, *Phys. Rev. Lett.* **8**, 250 (1962).
- <sup>35</sup>F. Lera, C. Rillo, R. Navarro, J. Bartolome, X. Obradors, J. Fontcuberta, X. Granados, M. Carrera, M. Vallet, J. Gonzalez-Calbert, J. Rodriguez, and M. Medarde, *Cryogenics* **29**, 379 (1989).
- <sup>36</sup>H. Kupfer, I. Apfelstedt, R. Flukiger, C. Keller, R. Meier-Hirmer, B. Runtzsch, A. Turowski, U. Weich, and T. Wolf, *Cryogenics* **29**, 268 (1989).
- <sup>37</sup>Yunhui Xu, Weiyan Guan, K. Zeibig, and C. Heiden, *Cryogenics* **29**, 281 (1989).
- <sup>38</sup>T. R. Finlayson, D. A. Garvie, D. B. Lowe, Z. Przelozny, and T. F. Smith, *Cryogenics* **30**, 467 (1990).
- <sup>39</sup>M. A.-K. Mohamed and J. Jung, *Phys. Rev. B* **44**, 4512 (1991).
- <sup>40</sup>C. W. Hagen and R. Griessen, *Phys. Rev. Lett.* **62**, 2857 (1989).
- <sup>41</sup>M. Reissner, W. Steiner, W. Kritschka, F. M. Sauerzopf, H. W. Weber, and G. W. Crabtree, *Physica C* **185-189**, 1819 (1991).
- <sup>42</sup>Ming Xu and Donglu Shi, *Physica C* **168**, 303 (1990).
- <sup>43</sup>Ming Xu, *Phys. Lett. A* **165**, 373 (1992).
- <sup>44</sup>L. Jansen and R. Block, *Physica C* **181**, 149 (1991).
- <sup>45</sup>S. Sridar, D. H. Wu, and W. Kennedy, *Phys. Rev. Lett.* **63**, 1873 (1989).
- <sup>46</sup>C. Ebner and D. Stroud, *Phys. Rev. B* **31**, 165 (1985).
- <sup>47</sup>Per Norling, Peter Svedlindh, Per Nordbald, Leif Lundgren, and Piotr Przyslupsky, *Physica C* **153-155**, 314 (1988).
- <sup>48</sup>F. Stuki, J. Rhyner, and G. Blatter, *Physica C* **181**, 385 (1991).
- <sup>49</sup>H. Jiang, A. Widom, Y. Huang, T. Yuan, C. Vittoria, D. B. Chrisey, and J. S. Horowitz, *Phys. Rev. B* **45**, 3048 (1992).
- <sup>50</sup>Samuel T. Weir, *Solid State Commun.* **77**, 839 (1991).
- <sup>51</sup>Ming Xu, Donglu Shi, A. Umezawa, K. G. Vandervoort, and G. W. Crabtree, *Phys. Rev. B* **43**, 13 049 (1991).
- <sup>52</sup>Z. Przelozny, T. R. Finlayson, D. A. Garvie, D. B. Lowe, and T. F. Smith, *Cryogenics* **31**, S433 (1991).
- <sup>53</sup>I. B. Khalifin, V. A. Larkin, B. Ya. Shapiro, and V. Oboznov, *Phys. Rev. B* **46**, 11 243 (1992).
- <sup>54</sup>N. Nakamura and M. Shimotomai, *Cryogenics* **31**, 379 (1991).
- <sup>55</sup>M. E. McHenry, M. P. Maley, G. H. Kwei, and J. D. Thompson, *Phys. Rev. B* **39**, 7339 (1989).
- <sup>56</sup>Hiroaki Kumakura, Kazumasa Togano, Eiji Yanagisawa, Kazuhiko Takahashi, Masao Nakao, and Hiroshi Maeda, *Jpn. J. Appl. Phys.* **28**, L24 (1989).
- <sup>57</sup>Antonio Barone, Anatoli I. Larkin, and Yuri N. Ovchinnikov, *J. Supercond.* **3**, 155 (1990).
- <sup>58</sup>M. W. McElfresh, Y. Yeshurun, A. P. Malozemoff, and F. Holtzberg, *Physica A* **168**, 308 (1990).
- <sup>59</sup>F. Lera, R. Navarro, C. Rillo, L. A. Angurel, A. Badia, and J. Bartolome, *J. Magn. Magn. Mater.* **104-107**, 615 (1992).
- <sup>60</sup>Du-Xing Chen and Alvaro Sanchez, *J. Appl. Phys.* **70**, 5463 (1991).
- <sup>61</sup>S. B. Ogale, D. Dijkamp, T. Venkatesan, X. D. Wu, and A. Inam, *Phys. Rev. B* **36**, 7210 (1987).